Journal of Applied Physics

Topological properties of coupled one-dimensional chains of elastic rotators

Cite as: J. Appl. Phys. **129**, 084903 (2021); https://doi.org/10.1063/5.0041256
Submitted: 21 December 2020 . Accepted: 13 February 2021 . Published Online: 25 February 2021

Pierre A. Deymier, Keith Runge, and M. Arif Hasan

AIP Publishing

Journal of Applied Physics ARTICLE scitation.org/journal/jap

Topological properties of coupled one-dimensional chains of elastic rotators

Cite as: J. Appl. Phys. **129**, 084903 (2021); doi: 10.1063/5.0041256
Submitted: 21 December 2020 · Accepted: 13 February 2021 ·
Published Online: 25 February 2021

Pierre A. Deymier,[a] Keith Runge,[b] and M. Arif Hasan[c]

AFFILIATIONS

Department of Materials Science and Engineering, University of Arizona, Tucson, Arizona 85721, USA

Note: This paper is part of the Special Topic on Acoustic Metamaterials 2021.
[a]**Author to whom correspondence should be addressed:** deymier@arizona.edu
[b]krunge@arizona.edu
[c]mdhasan@arizona.edu

ABSTRACT

We introduce a model system composed of elastically coupled one-dimensional chains of elastic rotators. The chains of rotators are analogous to elastic Su-Schrieffer–Heeger models. The coupled chain system is shown analytically and numerically to support an unusual number of topological properties such as Dirac degeneracies, band inversion and topological transition as a function of the strength of the parameter coupling the chains, nonseparability of the modes' degrees of freedom along and across the coupled chains that are analogous to entangled Bell states in a multipartite quantum system. Finally, we reveal the formation of a synthetic dimension by allowing the coupling parameter to vary with time, which has the potential to create higher-dimensional synthetic space.

I. INTRODUCTION

Recent advances in understanding the fundamental principles underlying the field of topological acoustics (TA) are beginning to nucleate a coherent body of knowledge. Simple one-dimensional (1D) phononic structures, analogous to the condensed matter Su-Schrieffer–Heeger (SSH) model, have revealed many of the fundamental properties of TA waves, such as topological invariance, edge states, and bulk-boundary correspondence.[1–5] In the SSH model, parity (P) symmetry is broken intrinsically through the system's structure. Spatiotemporal modulations of the elastic properties of 1D phononic structures can break time-reversal (T) and P symmetry.[6–10] However, numerous aspects of topological phenomena remain elusive including the notions of classical entanglement of TA waves and synthetic dimensions. Entangled states possess the two distinct attributes of nonlocality and nonseparability, whereas nonlocality is a unique feature of quantum mechanics, nonseparability is not. TA enables classical entanglement. Nonseparable elastic states, such as Bell states, have very recently been constructed in externally driven elastic systems as superpositions of elastic product states of two independent degrees of freedom.[11] In these driven systems, to complete the analogy with quantum Bell states (i.e., complexation of amplitudes), one exploits the dissipative nature (loss) of the constitutive materials. By tuning the complex amplitudes through the external drivers, one can experimentally navigate the Bell-state Hilbert space and execute quantum-like gates.[12] The dimension of the Hilbert space can increase through synthetic means (see below) or by exploiting nonlinearities. In the latter case, nonseparable inelastic modes can span exponentially complex Hilbert spaces.[13]

Topological properties have usually been demonstrated on spatial lattices with specifically engineered structural and geometrical features. Two- (2D) or three-dimensional (3D) TA systems exploit analogies with the quantum Hall effect (QHE),[14] quantum spin Hall effect (QSHE),[15] or quantum valley Hall effect (QVHE).[16] 2D TA systems use triangular lattice or graphene-like structures that exhibit Dirac point degeneracies in their band structure. Symmetry breaking then opens a gap associated with a nontrivial topology. Breaking symmetry intrinsically (e.g., P symmetry) leads to acoustic analogs of the QSHE or QVHE. Extrinsically breaking T symmetry results in acoustic analogs of the QHE. More recently, 3D acoustic and mechanical metamaterials have demonstrated Weyl points and Fermi arc-like surface states in Refs. 17–20. The propagation of edge states along sharp and curved interfaces (or surfaces) without backscattering has relied on the

bulk-boundary correspondence principle, a key characteristic of topologically ordered phases.[21] This correspondence states that the number of edge modes equals the difference in the Chern number between the abutting phases sharing the interface.

These prior studies focused onto topologically robust edge modes with higher-dimensional spatial lattices (e.g., to confine vibrations in a 1D guide, one must design 2D domains). Alternatively, nonspatial synthetic degrees of freedom offer a path to increase system dimensionality. Several approaches for creating such synthetic space dimensions have been explored in photonics.[22,23] Dynamic modulations of the optical properties of materials can be used to create modes at different frequencies and form an additional one-dimensional lattice in a synthetic frequency dimension. Furthermore, for systems described by a Hamiltonian dependent on some physical parameters, one can exploit the physical parameters as extra synthetic dimensions. The basic idea is to configure synthetic dimensions, and to combine such synthetic dimensions with the geometric dimensions to form a higher-dimensional synthetic space. Therefore, in contrast to traditional topological insulators with a spatial lattice, transport for topological waves in synthetic dimensions may occur at the edges of the synthetic space—not just a system's spatial edges.

In this paper, we consider a quasi-1D mechanical system for which there is extent in more than 1D. We introduce a model elastic system inspired by the electronic coupled SSH model. The topological phase diagram of two coupled SSH chains has been shown to be richer than that of a single SSH chain.[24] It exhibits a variety of trivial and nontrivial topological phases depending on the strength of the interchain and intrachain coupling. The application of the bulk boundary correspondence to predicting edge modes in the coupled SSH chain system has also been investigated.[25] The topological phase diagram of the coupled SSH system also shows fractal characteristics for quasiperiodic variation of couplings.[26]

Quasi-1D mechanical systems composed of periodic arrays of dimers coupled via springs have been shown to exhibit nontrivial topological characteristics, which can be generated by tuning the gyration radius of the dimer.[27] Topological band transition has been achieved in chains of cylindrical granular particles.[28] There, the transition is achieved by exploiting the tunability of Hertzian contact between particles. Finally, a 1-D system constituted of alternating unit cells composed of different 3D chiral micropolar metamaterials supports coupled longitudinal and rotational degrees of freedom reminiscent of a coupled SSH system.[29]

The present system is composed of two elastically coupled micromechanics SSH-like chains supporting rotational degrees of freedom. The two identical individual chains are translated with respect to each other by half their spatial period and elastically coupled along their length. The elastic stiffnesses of the two coupled chains are therefore out of registry spatially and the coupled system is built from two topologically distinct chains.[3] This system exhibits an unusual number of topological properties such as Dirac degeneracy, band inversion and topological transition, nonseparability of the modes degrees of freedom along and across the coupled chains and synthetic dimension in the form of the parameter coupling the chains. One of the novelties of this system resides in the possibility to tune its topological characteristics by changing the stiffness, which could be done practically and dynamically via non-contact methods.

We describe the model of coupled one-dimensional chains of elastic rotators in Sec. 2. Section 3 details the topological transition that the system undergoes upon changes in the strength of the elastic coupling. In Sec. 4, the nonseparability of the modes in the out of registry coupled system is contrasted with the separable modes of a model system where the chains are in registry. We show how the topological transition can be used to create quantum-like logic gates that operate on the nonseparable modes. Section 5 addresses analytically and numerically the use of the strength of the stiffness providing coupling between the chains as a parameter to form a higher-dimensional synthetic space and navigate the space of eigenmodes. Finally, conclusions are drawn in Sec. 6.

II. MODEL OF ELASTICALLY COUPLED CHAINS OF ROTATORS

In Fig. 1, we illustrate schematically the discrete linear one-dimensional (1D) micromechanics model that includes rotational degrees of freedom. This model is inspired by Cosserat-like lattice models.[30–32] It consists of two infinite chains of identical square block elements (rotator elements) connected with multiple harmonic springs. Positions along the chains are labeled as 2n−1, 2n, 2n+1, 2n+2, etc. The rotational axes of adjacent blocks are separated by the distance a. This system is periodic with a unit cell composed of four block elements (two in each chain). The period of the system along the chains is, therefore, $L = 2a$. Each block element has one rotational degree of freedom (rotation about an axis perpendicular to the plane of the figure). The rotational angles of elements in the top chain and bottom chain are labeled as, u_i and v_i with i=…, 2n−1, 2n, 2n+1, 2n+2, …, respectively. All block elements are identical with positive moment of inertia, m.

The elements are connected to each other by their corners via linear springs. Within a given chain, the corners of even elements are elastically linked to the opposite corners of odd elements to their left, thus, forming X-shaped connections. The corners of even elements are linked to the corresponding corners of odd elements to their right, forming a set of two horizontal parallel connections. Between the two chains, elements are coupled elastically via vertical

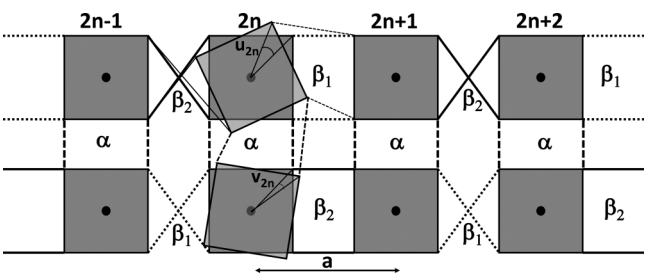

FIG. 1. Schematic illustration of two one-dimensional chains of rotators coupled elastically along their length. The figure shows the 2n blocks undergoing rotations with the corresponding rotational degrees of freedom. See the text for details and meaning of symbols.

parallel connections. The stiffness of the vertical parallel connections is α.

The X-shaped connections in the top and bottom chains have different stiffnesses, β_2 and β_1. The parallel connections in the top and bottom chains have also different stiffnesses, namely, β_1 and β_2. The alternating stiffnesses of the two chains are out of registry along the chains, i.e., a connection with a stiffness β_1 in the upper chains sees a connection with stiffness β_2 in the lower chain. Similar to SSH models, the uncoupled individual chains with stiffnesses out of registry are topologically distinct.[3] The Berry phase of two individual chains translated by half a spatial period relative to each other differs by π.[3]

In the limit of small rotational angles and hence for linear elasticity (i.e., β_1 β_2 fixed), the potential energy associated with the X connections in the upper chain is given by $E_{2n-1,2n} = 1/2\beta_2(u_{2n-1} + u_{2n})^2$. In the lower chain, the potential energy of X-shaped connections is expressed in a similar form as $E_{2n-1,2n} = 1/2\beta_1(v_{2n-1} + v_{2n})^2$. The elastic energy of horizontal parallel connections in the upper and lower chains are $E_{2n,2n+1} = 1/2\beta_2(u_{2n} - u_{2n+1})^2$ and $E_{2n,2n+1} = 1/2\beta_2(v_{2n} - v_{2n+1})^2$. Finally, the elastic energy of vertical parallel connections between elements of the two chains is expressed as $E_{2n,2n} = 1/2\alpha(u_{2n} - v_{2n})^2$.

The rotational equations of motion of the coupled chains of rotators take the form

$$m\frac{\partial^2 u_{2n}}{\partial t^2} = -\beta_2(u_{2n-1} + u_{2n}) - \beta_1(u_{2n} - u_{2n+1}) + \alpha(v_{2n} - u_{2n}), \tag{1a}$$

$$m\frac{\partial^2 u_{2n+1}}{\partial t^2} = \beta_1(u_{2n} - u_{2n+1}) - \beta_2(u_{2n+1} + u_{2n+2}) + \alpha(v_{2n+1} - u_{2n+1}), \tag{1b}$$

$$m\frac{\partial^2 v_{2n}}{\partial t^2} = -\beta_1(v_{2n-1} + v_{2n}) - \beta_2(v_{2n} - v_{2n+1}) - \alpha(v_{2n} - u_{2n}), \tag{1c}$$

$$m\frac{\partial^2 v_{2n+1}}{\partial t^2} = \beta_2(v_{2n} - v_{2n+1}) - \beta_1(v_{2n+1} + v_{2n+2}) - \alpha(v_{2n+1} - u_{2n+1}). \tag{1d}$$

We choose the following Ansatz to solve these equations: $u_{2n} = A_1 e^{ik2na}e^{i\omega t}$, $u_{2n+1} = A_2 e^{ik(2n+1)a}e^{i\omega t}$, $v_{2n} = B_1 e^{ik2na}e^{i\omega t}$, and $v_{2n+1} = B_2 e^{ik(2n+1)a}e^{i\omega t}$, where k and ω are the wave vector and angular frequency, respectively. With this, Eqs. (1a), (1b), (1c), and (1d) reduce to an eigenproblem of the form

$$\overleftrightarrow{D}\vec{A} = 0, \tag{2}$$

where

$$\overleftrightarrow{D} = \begin{pmatrix} \gamma & -\delta & -\alpha & 0 \\ -\delta^* & \gamma & 0 & -\alpha \\ -\alpha & 0 & \gamma & \delta^* \\ 0 & -\alpha & \delta & \gamma \end{pmatrix} \quad \text{and} \quad \vec{A} = \begin{pmatrix} A_1 \\ A_2 \\ B_1 \\ B_2 \end{pmatrix},$$

with $\gamma = -m\omega^2 + \beta_1 + \beta_2 + \alpha$ and $\delta = \beta_1 e^{+ika} - \beta_2 e^{-ika}$. δ^* is the complex conjugate of δ.

Equation (2) has non-trivial solutions if the determinant of the dynamical matrix is equal to zero. This condition gives the solutions of a quadratic equation $\gamma^2 - \delta\delta^* = \alpha^2 \pm \alpha\sqrt{-(\delta - \delta^*)^2}$ with $\delta - \delta^* = 2i(\beta_1 + \beta_2)\sin ka$ and $\delta\delta^* = \beta_1^2 + \beta_2^2 - 2\beta_1\beta_2\cos 2ka$. The four dispersion relations (corresponding to the different combinations of signs, $\pm$ in front of the square root and possible sign of $\sqrt{\gamma^2}$, $[\pm]$) are then obtained in the form

$$m\omega^2 = \beta_1 + \beta_2 + \alpha[\pm]\sqrt{\beta_1^2 + \beta_2^2 - 2\beta_1\beta_2\cos 2ka + \alpha^2 \pm 2\alpha(\beta_1 + \beta_2)|\sin ka|}. \tag{3}$$

Here, we have used the symbol $[\pm]$ to differentiate the two $\pm$ in Eq. (3). Bands and modes will subsequently be differentiated by the couple in the parenthesis ($[\pm]$, $\pm$). When $\alpha = 0$, this dispersion relation reduces to that of uncoupled chains. These chains are the rotator equivalent of the 1D SSH model reported in Ref. 3 with the band structure translated in wave number space by $\pi/2$.

Since the periodicity of the coupled chain system is $L = 2a$, The Brillouin zone (BZ) extends over the range $k \in [-\pi/L, \pi/L]$, i.e., $ka \in [-\pi/2, \pi/2]$. Equation (3) is indeed π periodic. However, in that representation, the dispersion relations are not representative of the eigenmodes across the origin $ka = 0$ as the group velocity ($\partial\omega/\partial k$) given by Eq. (3) is not continuous across the origin $ka = 0$. To calculate the eigenvectors, we reformulate the dispersion relations as the extended relations

$$m\omega^2 = \beta_1 + \beta_2 + \alpha[\pm]\sqrt{\beta_1^2 + \beta_2^2 - 2\beta_1\beta_2\cos 2ka + \alpha^2 \pm 2\alpha(\beta_1 + \beta_2)\sin ka}. \tag{4}$$

Bands intersect two by two at the origin forming two Dirac points were the dispersion relations cross linearly in the vicinity of the origin.

Individual extended dispersion relations given by Eq. (4) exhibit periodicity over the interval $ka \in [-\pi, \pi]$ and are continuously representative of the eigenmodes. To solve for the eigenvectors, we rewrite Eq. (2) as the set of two coupled equations

$$\begin{pmatrix} \gamma & -\delta \\ -\delta^* & \gamma \end{pmatrix}\begin{pmatrix} A_1 \\ A_2 \end{pmatrix} = \alpha\overleftrightarrow{I}\begin{pmatrix} B_1 \\ B_2 \end{pmatrix}, \tag{5a}$$

$$\begin{pmatrix} \gamma & \delta^* \\ \delta & \gamma \end{pmatrix} \begin{pmatrix} B_1 \\ B_2 \end{pmatrix} = \alpha \overleftrightarrow{I} \begin{pmatrix} A_1 \\ A_2 \end{pmatrix}, \tag{5b}$$

where $\overleftrightarrow{I}$ is the 2×2 identity matrix.

Combining these two equations, we obtain the following equation for $\begin{pmatrix} A_1 \\ A_2 \end{pmatrix}$:

$$\begin{pmatrix} \gamma^2 - \delta^{*2} - \alpha^2 & -\gamma(\delta - \delta^*) \\ \gamma(\delta - \delta^*) & \gamma^2 - \delta^2 - \alpha^2 \end{pmatrix} \begin{pmatrix} A_1 \\ A_2 \end{pmatrix} = 0. \tag{6}$$

Choosing $A_2 = A_1^*$ shows that the two equations forming Eq. (6) are complex conjugate of each other and are therefore equivalent. Thus, Eq. (6) reduces to the single linear relation

$$(\gamma^2 - \delta^{*2} - \alpha^2)A_1 = \gamma(\delta - \delta^*)A_2. \tag{7}$$

We have, $\gamma^2 - \delta^{*2} - \alpha^2 = \delta^*(\delta - \delta^*) \pm \alpha\sqrt{-(\delta - \delta^*)^2}$. Using the extended dispersion relation where $\sqrt{-(\delta - \delta^*)^2}$ is taken as $2(\beta_1 + \beta_2)\sin ka$ (i.e., without the absolute value), Eq. (7) becomes $Z^* 2(\beta_1 + \beta_2)\sin kaA_1 = \gamma 2i(\beta_1 + \beta_2)\sin kaA_2$ where $Z^* = i\delta^* \pm \alpha$. We can simplify this equation for all $ka \neq 0$, leading to the relation

$$Z^* A_1 = i\gamma A_2. \tag{8}$$

If $ka = 0$, the bands cross and form a degenerate point. The solution to the eigenvector problem is not a single mode but a superposition of degenerate eigenmodes.

We also note that in the extended dispersion relation representation $\gamma^2 = \delta\delta^* + \alpha^2 \pm (-i)\alpha(\delta - \delta^*) = ZZ^*$, i.e., $\gamma = [\pm]\sqrt{Z}\sqrt{Z^*}$. We have used $[\pm]$ introduced earlier. Finally, we can simplify Eq. (8) to a form involving two complex conjugate coefficients,

$$\sqrt{-i}\sqrt{Z^*}A_1 = [\pm]\sqrt{i}\sqrt{Z}A_2. \tag{9}$$

We, therefore, take to within a complex constant: $A_1 = [\pm]\sqrt{i}\sqrt{Z}$ and $A_2 = \sqrt{-i}\sqrt{Z^*}$. Inserting these expressions in Eq. (5a), we obtain to within the same constant $B_1 = \pm\sqrt{i}\sqrt{Z^*}$ and $B_2 = \pm[\pm]\sqrt{-i}\sqrt{Z}$.

We can now obtain the normalized eigenvector $\overrightarrow{\hat{A}}$,

$$\overrightarrow{\hat{A}} = \frac{1}{2\sqrt{\sqrt{Z}\sqrt{Z^*}}} \begin{pmatrix} [\pm]\sqrt{i}\sqrt{Z} \\ \sqrt{-i}\sqrt{Z^*} \\ \pm\sqrt{i}\sqrt{Z^*} \\ \pm[\pm]\sqrt{-i}\sqrt{Z} \end{pmatrix}. \tag{10}$$

The complete normalized displacement vector Ansatz is, therefore,

$$\overrightarrow{\hat{u}} = \frac{1}{2\sqrt{\sqrt{Z}\sqrt{Z^*}}} \begin{pmatrix} [\pm]\sqrt{i}\sqrt{Z}e^{ik2na} \\ \sqrt{-i}\sqrt{Z^*}e^{ik(2n+1)a} \\ \pm\sqrt{i}\sqrt{Z^*}e^{ik2na} \\ \pm[\pm]\sqrt{-i}\sqrt{Z}e^{ik(2n+1)a} \end{pmatrix} e^{i\omega t}.$$

The topological characteristics of these eigenvectors are discussed in subsequent sections.

III. BAND INVERSION AND TOPOLOGICAL TRANSITION

In Fig. 2, we have plotted the four individual extended dispersion relations given by Eq. (4) over the interval $ka \in [-\pi, \pi]$. At the positive edge of the BZ, the dispersion relation simplifies to

$$m\omega^2 = \beta_1 + \beta_2 + \alpha[\pm](\beta_1 + \beta_2 \pm \alpha).$$

For the sake of illustration, choosing the bands $([\pm], -)$, $m\omega^2$ takes on two values, $2(\beta_1 + \beta_2)$ for the mode $([+], -)$ or 2α for the mode $([-], -)$. We also remark that as $\alpha = \beta_1 + \beta_2$, the two bands corresponding to these two modes touch at the BZ edges. When $\alpha < \beta_1 + \beta_2$, the lower band corresponds to the mode $([-], -)$, and the upper band corresponds to the modes $([+], -)$. For $\alpha > \beta_1 + \beta_2$, the lower band is now a representative of the mode $([+], -)$ and the upper band corresponds to the mode $([-], -)$. A similar behavior occurs for the other two bands at the negative edge of the BZ. The band structure exhibits a band inversion. As we will see when considering the eigenmodes, the band inversion between upper and lower bands leads to a topological transition.

In Fig. 3, we have plotted the complex quantities in the normalized eigenvectors, $y_1 = \sqrt{i}\sqrt{Z}/2\sqrt{\sqrt{Z}\sqrt{Z^*}}$, $y_2 = \sqrt{-i}\sqrt{Z^*}/2\sqrt{\sqrt{Z}\sqrt{Z^*}}$, $y_3 = \sqrt{i}\sqrt{Z^*}/2\sqrt{\sqrt{Z}\sqrt{Z^*}}$, and $y_4 = \sqrt{-i}\sqrt{Z}/2\sqrt{\sqrt{Z}\sqrt{Z^*}}$ corresponding to $Z^* = i\delta^* - \alpha$ and $Z = -i\delta - \alpha = (\beta_1 + \beta_2)\sin x - \alpha + i(\beta_1 - \beta_2)\cos x$ as functions of $x = ka$. We are considering two values of the parameter α below and above $\beta_1 + \beta_2$, respectively. When $\alpha < \beta_1 + \beta_2$, we note that the real and imaginary parts of all the components exhibit a discontinuity at the lower edge of the BZ ($x = -\pi/2$). At the upper edge of the BZ, both real and imaginary parts are varying continuously. In contrast, for $\alpha > \beta_1 + \beta_2$, the real and imaginary parts of the four components show two discontinuities at both edges of the BZ $\left(x = -\frac{\pi}{2}, +\frac{\pi}{2}\right)$. These features are indicative of a topological transition. Since the coupled chain system studied here is infinite, to quantify the topology of the eigenmodes, we calculate the Berry connection and Berry phase of the normalized eigenvector, $\overrightarrow{\hat{u}}$, corresponding to a particular band in the band structure.[33] The geometric phase that characterizes the property of bulk bands in periodic systems is also known as the Zak phase.[34] The displacement unit vector evolves along some parametric curve as x is varied. The Berry connection characterizes the variation in orientation of the unit vector along some path in the complex space of amplitudes parametrized by x. The evolution of the normalized amplitude vector in the multidimensional space parametrized by the wave number k (or $x = ka$) generates a manifold. The Berry phase is the net phase accumulated by the amplitude unit vector over the entire manifold for a closed path. That is to say, the Berry phase characterizes the topology of the manifold.

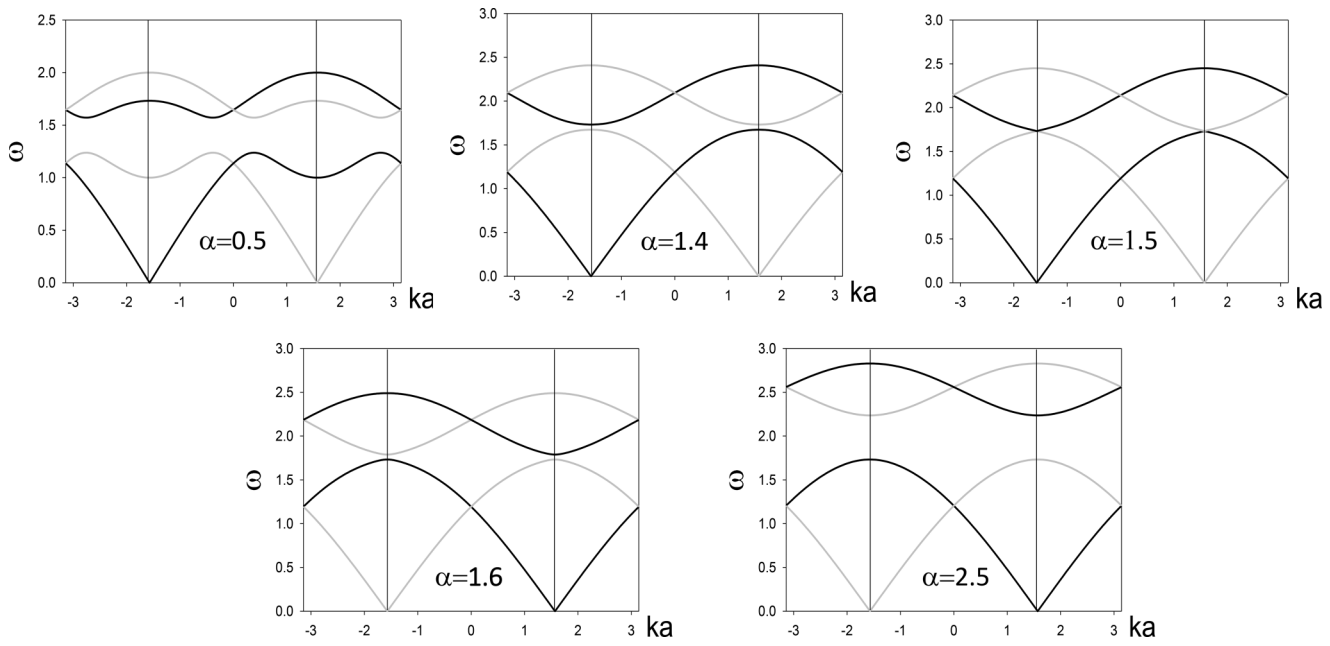

FIG. 2. Evolution of the band structure as a function of the coupling stiffness α. Here, we have chosen $\beta_1 = 1$, $\beta_2 = 0.5$, $m = 1$. Black and gray lines are used to represent the different bands ($[\pm]$, $\pm$) given by Eq. (4) to highlight the band inversion at $\alpha = \beta_1 + \beta_2 = 1.5$. The dispersion relations are plotted over the interval $ka \in [-\pi,\ \pi]$. The Brillouin zone extends over the range $ka \in [-\pi/2, \pi/2]$ and is delimited by vertical lines.

The Berry connection, BC, is calculated in the case of continuous displacement vectors as $BC(x) = -i\,\vec{\hat{u}}^{\dagger}\,\partial\,\vec{\hat{u}}\,/\partial x$, which leads to

$$BC(x) = -i\,\vec{\hat{A}}^{\dagger}\frac{\partial\,\vec{\hat{A}}}{\partial x} + \text{const.} \tag{11}$$

The constant term comes from the $x = ka$ dependency of the terms e^{ik2na} and $e^{ik(2n+1)a}$. This term only adds the same constant phase to the geometric phase of the different bands.

In the first term of Eq. (11), $\vec{\hat{A}}^{\dagger}$, is the Hermitian conjugate of $\vec{\hat{A}}$. Application of Eq. (11) to the normalized eigenamplitude vector of Eq. (10) implies the calculation of the following terms: $T_1 = \partial f(x)/\partial x$ and $T_2 = \partial f^{*}(x)/\partial x$, where $f(x) = \sqrt{Z}/2\sqrt{\sqrt{Z}\sqrt{Z^{*}}}$. The continuous form of the Berry connection becomes: $BC(x) = 2(f^{*}(x)\partial f(x)/\partial x + f(x)^{*}(x)/\partial x)$, which can be shown to vanish. This is true irrespective of the sign $[\pm]$. The continuous parts of the normalized amplitude vector do not contribute to the Berry connection.

The contribution to the Berry phase of the discontinuities of the normalized eigenmodes at the edge of the BZ, can be calculated as follows:

$$\phi_{BC} = -\text{Im}\left\{\ln\left[\lim_{\varepsilon\to 0}\vec{\hat{A}}^{\dagger}(x_{dis}-\varepsilon)\,\vec{\hat{A}}(x_{dis}+\varepsilon)\right]\right\}. \tag{12}$$

In Eq. (12), Im takes the imaginary part of its argument, x_{dis} is the location of the discontinuity. The argument of the ln function in Eq. (12) takes the form

$$\lim_{\varepsilon\to 0}\vec{\hat{A}}^{\dagger}(x_{dis}-\varepsilon)\,\vec{\hat{A}}(x_{dis}+\varepsilon) = \lim_{\varepsilon\to 0}\left\{\sum_{j=1}^{4} y_j^{*}(x_{dis}-\varepsilon)y_j(x_{dis}+\varepsilon)\right\},$$

where y_j's were defined earlier. This expression does not depend on the sign $[\pm]$ since the product $[\pm][\pm]$ is always positive. As seen in Fig. 3, for each discontinuity at an edge of the BZ, the imaginary part of a y_j is of opposite sign compared to the real part, so we define $\lim_{\varepsilon\to 0} y_j(x_{dis}+\varepsilon) = a_j - ib_j$. On the other side of the discontinuity, the signs of the real and imaginary parts are inverted, so $\lim_{\varepsilon\to 0} y_j(x_{dis}-\varepsilon) = -a_j + ib_j$, and therefore, $\lim_{\varepsilon\to 0} y_j^{*}(x_{dis}-\varepsilon) = -a_j - ib_j$. With this,

$$\lim_{\varepsilon\to 0}\left\{\sum_{j=1}^{4} y_j^{*}(x_{dis}-\varepsilon)y_j(x_{dis}+\varepsilon)\right\} = -\sum_{j=1}^{4}(a_j^2+b_j^2),$$

which is always a negative real quantity. Inserting this expression in Eq. (12) results in

$$\begin{aligned}\phi_{BC} &= -\text{Im}\left\{\ln\left[-\sum_{j=1}^{4}(a_j^2+b_j^2)\right]\right\}\\ &= -\text{Im}\left\{\ln(-1) + \ln\left[\sum_{j=1}^{4}(a_j^2+b_j^2)\right]\right\}.\end{aligned}$$

Since $\ln(-1) = \ln(e^{\pm i\pi}) = \pm i\pi$, the Berry connection associated with one discontinuity of the amplitude unit vector is $\phi_{BC} = \mp\pi$. When $\alpha < \beta_1 + \beta_2$, the components of the amplitude unit vector exhibit a single discontinuity. The Berry phase in that case is $\mp\pi$. When $\alpha > \beta_1 + \beta_2$, the components of the amplitude unit vector show two discontinuities. Each discontinuity contributes $\mp\pi$ to the Berry phase. The total Berry phase is therefore 0 or 2π. A topological transition is taking place at $\alpha = \beta_1 + \beta_2$, with two topologically different eigenmodes on both sides of this transition point. The modes corresponding to the lower and upper bands in the band structure undergo this topological transition simultaneously.

IV. NONSEPARABILITY OF EIGENMODES

The system composed of the two chains with stiffnesses out of registry investigated in Secs. 2 and 3, exhibit eigenmodes that are not separable. That is, the 4×1 eigenvector cannot be written as a single tensor product of two 2×1 vectors. This is in contrast with a related system whereby the stiffnesses along the two chains are in registry (see the Appendix). Let us repeat the normalize amplitude vector of Eq. (10),

$$\vec{\hat{A}} = \begin{pmatrix} [\pm]y_1 \\ y_2 \\ \pm y_3 \\ \pm[\pm]y_4 \end{pmatrix}.$$

This vector cannot be written as a single tensor product but as a linear combination of tensor products,

$$\vec{\hat{A}} = [\pm]y_1 \begin{pmatrix} 1 \\ 0 \end{pmatrix}_u \otimes \begin{pmatrix} 1 \\ 0 \end{pmatrix}_c + y_2 \begin{pmatrix} 0 \\ 1 \end{pmatrix}_u \otimes \begin{pmatrix} 1 \\ 0 \end{pmatrix}_c \pm y_3 \begin{pmatrix} 1 \\ 0 \end{pmatrix}_u \otimes \begin{pmatrix} 0 \\ 1 \end{pmatrix}_c \pm [\pm] y_4 \begin{pmatrix} 0 \\ 1 \end{pmatrix}_u \otimes \begin{pmatrix} 0 \\ 1 \end{pmatrix}_c. \tag{13}$$

In Eq. (13), $\left\{ \begin{pmatrix} 1 \\ 0 \end{pmatrix}_p, \begin{pmatrix} 0 \\ 1 \end{pmatrix}_p \right\}$ forms a basis in the two-dimensional (2D) Hilbert space, P, of position along a chain within the unit cell. $\left\{ \begin{pmatrix} 1 \\ 0 \end{pmatrix}_c, \begin{pmatrix} 0 \\ 1 \end{pmatrix}_c \right\}$ forms a basis in the 2D Hilbert space, C, of the chains (top or bottom). Products of the form $\begin{pmatrix} 0 \\ 1 \end{pmatrix}_p \otimes \begin{pmatrix} 1 \\ 0 \end{pmatrix}_c$ constitute a basis in the four-dimensional (4D) product Hilbert space $P \otimes C$. The amplitude vector, $\vec{\hat{A}}$, is not separable in that space, a classical attribute of entangled states.

Below we illustrate how the parameter α can be used to navigate the 4D Hilbert space. Let us choose a mode corresponding to a defined band inside the BZ but at its positive edge, i.e., $x = \pi^-/2$. From Fig. 3, we note that for $\alpha = 1.45$, to within the same real constant $(1/2\sqrt{2})$, $y_1 = \sqrt{i}$, $y_2 = \sqrt{-i}$, $y_3 = \sqrt{i}$, and $y_4 = \sqrt{-i}$. For $\alpha = 1.55$, we have to within the same real constant, $y_1' = -\sqrt{-i}$, $y_2' = -\sqrt{i}$, $y_3' = \sqrt{-i}$, and $y_4' = \sqrt{i}$. So upon a transition from $\alpha = 1.45$ to 1.55, the unit amplitude vectors change from: $\vec{\hat{A}} = 1/2\sqrt{2}\left([\pm]\sqrt{i} \quad \sqrt{-i} \quad \pm\sqrt{i} \quad \pm[\pm]\sqrt{-i} \right)$ to $\vec{\hat{A}'} = 1/2\sqrt{2}\left([\mp](-1)\sqrt{-i} \quad -\sqrt{i} \quad \pm\sqrt{-i} \quad \pm[\mp]\sqrt{i} \right)$. The $[\mp]$ in the expression for $\vec{\hat{A}'}$ comes from the effect of band inversion; the sign changes for the mode to remain on the same band (see Sec. 3). This is an *intra*band transition. These two vectors are related to each other by the unitary transformation, $\overleftrightarrow{U}$: $\vec{\hat{A}'} = \overleftrightarrow{U}\vec{\hat{A}}$ which can be defined as

$$\frac{1}{2\sqrt{2}} \begin{pmatrix} [\mp](-1)\sqrt{-i} \\ -\sqrt{i} \\ \pm\sqrt{-i} \\ \pm[\mp]\sqrt{i} \end{pmatrix} = \begin{pmatrix} 0 & [\pm]1 & 0 & 0 \\ -[\pm]1 & 0 & 0 & 0 \\ 0 & 0 & 0 & [\pm]1 \\ 0 & 0 & -[\pm]1 & 0 \end{pmatrix} \frac{1}{2\sqrt{2}} \begin{pmatrix} [\pm]\sqrt{i} \\ \sqrt{-i} \\ \pm\sqrt{i} \\ \pm[\pm]\sqrt{-i} \end{pmatrix}.$$

We rewrite $\overleftrightarrow{U} = [\pm]\sigma_y \otimes i\overleftrightarrow{I} = [\pm]\begin{pmatrix} 0 & -i \\ i & 0 \end{pmatrix} \otimes i\begin{pmatrix} 1 & 0 \\ 0 & 1 \end{pmatrix}$, where σ_y is one of the three Pauli matrices. The topological transition is equivalent to an operation that enables us to navigate the 4D product Hilbert space of amplitudes. $\overleftrightarrow{U}$ is isomorphic to applying a Pauli-Y quantum logic gate, following the application of a general phase shift of $\pi/2$. The Pauli-Y gate is equivalent to a rotation about the Y axis of the Bloch sphere by π.

Now if we allow a transition between bands from mode $\vec{\hat{A}}$ to a mode $\vec{\hat{A}}''$ $= 1/2\sqrt{2}\left([\pm](-1)\sqrt{-i} \quad -\sqrt{i} \quad \pm\sqrt{-i} \quad \pm[\pm]\sqrt{i}. \right)$. The *inter*band transition conserves $[\pm]$. These two vectors are now related to each other by the unitary transformation $\overleftrightarrow{U} = -\sigma_x \otimes \sigma_z = -\begin{pmatrix} 0 & 1 \\ 1 & 0 \end{pmatrix} \otimes \begin{pmatrix} 1 & 0 \\ 0 & -1 \end{pmatrix}$, where σ_x and σ_z are the Pauli-X and Pauli-Z matrices. Note that the variation from one

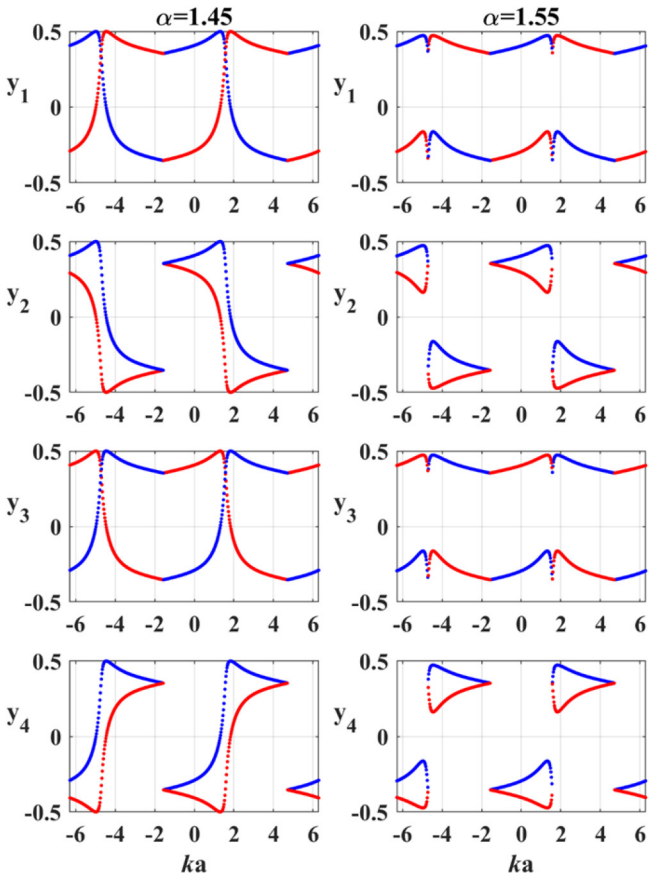

FIG. 3. Complex components of the normalized eigenvectors, y_1, y_2, y_3, and y_4 (top to bottom), as functions of $x = ka$. We have chosen $\beta_1 = 1$, $\beta_2 = 0.5$ (i.e., $\beta_1 + \beta_2 = 1.5$), and $m = 1$. $\alpha = 1.45 < 1.5$ and $\alpha = 1.55 > 1.5$. The blue curves are the real part of the complex components. The red curves are the imaginary part. x extends beyond the first BZ to clearly display the nature of the discontinuities.

value of α to another across the topological transition value $\alpha = \beta_1 + \beta_2$ would, in general, require a change of frequency at a fixed wave number. This point is further discussed in the next section.

Finally, we also remark that away from the edges of the BZ (i.e., in the vicinity of the center of the BZ where modes do not exhibit discontinuities), as can be seen in Fig. 3, transitioning α across the topological transition does not change significantly the y_i's. An *intra*band transition would convert the vector $\vec{A} = (\,[\pm]y_1 \quad y_2 \quad \pm y_3 \quad \pm[\pm]y_4\,)$ into $\vec{A'} = (\,[\mp]y_1 \quad y_2 \quad \pm y_3 \quad \pm[\mp]y_4\,)$ with a unitary transformation $\overleftrightarrow{U} = -\sigma_z \otimes \sigma_z$. An *inter*band transition produces $\vec{A}'' = \vec{A}$ with the identity matrix as the transformation matrix.

V. SYNTHETIC DIMENSION

A common method to create a synthetic space is to utilize the parameter degrees of freedom of a system. The physical parameter α can serve as such a degree of freedom. The equations of motion [Eqs. (1a), (1b), (1c), and (1d)] are parametrically dependent on α, which can be treated as a continuous variable. The dependency of the system can then be described in a synthetic space with a α axis playing the role of an extra synthetic dimension in addition to time (or ω) and position (or $x = ka$). Topological effects such as the topological transition presented earlier naturally arise in such a synthetic space.

Complex components of the normalized eigenvectors, y, as functions of $x = ka$. We have chosen $\beta_1 = 1$, $\beta_2 = 0.5$ (i.e., $\beta_1 + \beta_2 = 1.5$), and $m = 1$. $\alpha = 1.45 < 1.5$ and $\alpha = 1.55 > 1.5$. The blue lines are the real part of the complex components. The red lines are the imaginary part.

In Fig. 4, for the sake of illustration, we plot $y_1 = \sqrt{i}\sqrt{Z}/2\sqrt{\sqrt{Z}\sqrt{Z^*}}$ as a function of x and α. Since $\pm$ in $Z^* = i\delta^* \pm \alpha$ and $Z = -i\delta \pm \alpha$ correspond to two different bands (either the lower two or upper two bands), in Fig. 4, a negative α corresponds to one band, $([\pm], -)$, and a positive α to the other one, $([\pm], +)$. Choosing $\alpha < -1.5$, the figure shows two discontinuities as a function of x. For $1.5 > \alpha > -1.5$, y_1 exhibits only one discontinuity as a function of x. This is identical to Fig. 3. Considering, the other band in the case of positive α, if $1.5 > \alpha > 0$, $y_1(x)$ shows only one discontinuity. For $\alpha > 1.5$, there is no discontinuity. This is again the signature of a topological transition with a change of Berry phase of π.

We observe that there is no discontinuity in y_1 as a function of α but at the edges of the BZ. Considering only the $([\pm], -)$ bands, that is, $\alpha < 0$, at $x = \pi^-/2$, there is a discontinuity in y_1 at $\alpha = -1.5$. Across that discontinuity y_1 changes from $1/2\sqrt{2}\sqrt{i}$ to $1/2\sqrt{2}\sqrt{-i}$ as was shown in Sec. 4. Therefore, the amplitude unit vectors within the same band are related to each other through the unitary transformation $\overleftrightarrow{U} = \sigma_y \otimes i\overleftrightarrow{I}$, as was seen earlier.

On one hand, we may consider the coupled one-dimensional chains of elastic rotators with varying values of the coupling parameter as an ensemble of different physical systems. On the other hand, by allowing the coupling parameter to vary as a function of time, we can navigate the two-dimensional synthetic space with one single physical system. The ability to dynamically tune the stiffness of the coupling between the chains of rotators is key to enabling the exploration of the synthetic dimension. Non-contact experimental methods shown to induce changes in elastic stiffness can leverage various forms of electromagnetic-elastic coupling.[35–38] In addition to magneto-elastic effects and piezoelectric effects, fast and reversible changes in elastic stiffness can also be achieved by applying light-induced thermal stimulation of phase change materials (PCMs) used in modern information technologies.[39]

To illustrate the properties of the chain of rotators with time varying coupling, we simulate the effect of a rapid change of the coupling parameter α. This is analogous to scattering by a time discontinuity or time interface.[40–42] Scattering by a time interface transforms the wave prior to the change into two waves possessing different but opposite frequencies while conserving the wave number. We develop a numerical model based on coupled chains of elastic rotators as shown in Fig. 1. We use Born–von Karman periodic boundary conditions for which $e^{ikN_cL} = 1$; N_c is the total number of unit cells along the chains. As mentioned above, in the first BZ, ka is limited to the interval $-\pi/2$ to $\pi/2$ with a spacing of

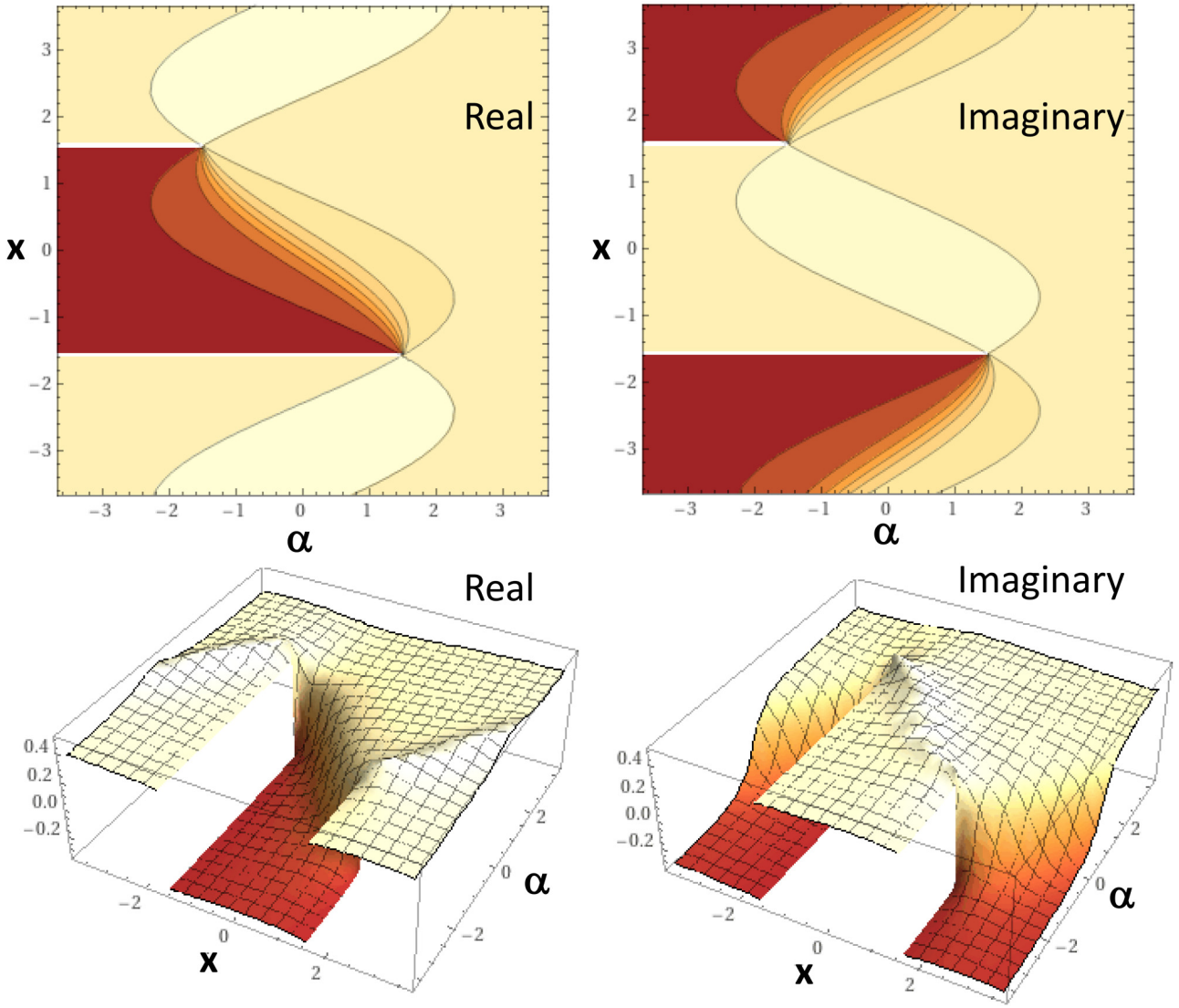

FIG. 4. Contour plots and 3D plots of the real and imaginary parts of $y_1 = \sqrt{i}\sqrt{Z}/2\sqrt{\sqrt{Z}\sqrt{Z^*}}$ as a function of x and α. The darker colors correspond to negative values and the lighter colors to positive values. We have chosen $\beta_1 = 1$, $\beta_2 = 0.5$ (i.e., $\beta_1 + \beta_2 = 1.5$), and $m = 1$.

$2\pi/N_c$. A vectorized fourth order Runge–Kutta time integration scheme is used to numerically calculate the dynamics of system.

Using the computational tool for the spectral analysis of amplitudes and phases (SAAP) of elastic waves,[3] we excite a single eigenmode of the second branch at the positive side of the BZ (that is, band $([-], -)$) by introducing local phase values as part of the initial condition. We investigate the effect of the time varying coupling for two wave numbers: (i) at $ka = \pi/4$, value away from the edge of the BZ, and (ii) at $ka = \pi/2$ on the edge of the BZ. Furthermore, we run the numerical simulation a total of 2^{18} time steps, while keeping the initial coupling parameter α_i for the first 2^{17} time steps and then rapidly changing α to the final value, α_f, and maintaining this value during the next 2^{17} time steps. We record and Fourier transform the time dependency of the displacement of a representative rotator in the top chain during this second time interval. We consider two time interfaces, one that crosses the band inversion value, $\beta_1 + \beta_2$, and another one whereby α_i, α_f remain both below the inversion value. In Fig. 5, we show the power spectral density of the representative block element's amplitude calculated over the 2^{17} time steps after the rapid change in coupling stiffness.

From Fig. 5(a), it is clear that by choosing a wave number, $ka = \pi/4$, away from the edge of the BZ, scattering by a time interface transforms an earlier wave of frequency $\omega_i = 1.156$ into a

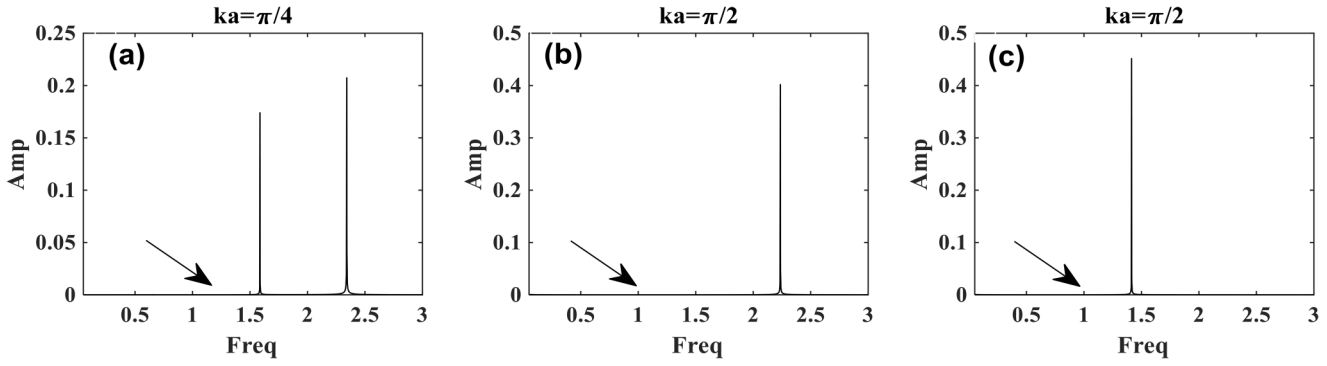

FIG. 5. Power spectral density of the displacement of a representative rotator in the top chain, showing the eigenfrequencies. Arrows indicate the initial excitation frequency (ω_i) of the input eigenmode: (a) $\omega_i = 1.156$ and $(\alpha_i, \alpha_f) = (0.5, 2.5)$, (b) $\omega_i = 1.0$ and $(\alpha_i, \alpha_f) = (0.5, 2.5)$, (c) $\omega_i = 1.0$ and $(\alpha_i, \alpha_f) = (0.5, 1.0)$. System parameters $N_c = 12$, $N_m = 2$, $\beta_1 = 0.5$, $\beta_2 = 1.0$.

superposition of two sets of waves with corresponding final frequency (ω_f) values of $\omega_{f,1} = 1.587$ (corresponding to an *intra*band transition) and $\omega_{f,2} = 2.342$ (corresponding to an *inter*band transition). These two sets of waves have the same wave number as that of the earlier wave. We note that because of the finite size of the simulated systems as well as of the periodic boundary conditions, it is not possible numerically to differentiate between positive and negative frequency waves. On the other hand, if we choose $ka = \pi/2$ at the edge of the BZ [as shown in Fig. 5(b)], scattering by a time interface only transforms an earlier wave of frequency $\omega_i = 1.0$ to a later single mode of frequency $\omega_f = 2.236$. This transition takes place between two different bands. These transitions are illustrated graphically in Fig. 6. If we take α_f to be 1.0, Fig. 5(c) shows that the scattered wave (with frequency $\omega_f = 1.414$) corresponds to the same band as that of the early wave. Hence, choosing a wave number value at the edge of the BZ allows us to achieve a single mode conversion via scattering by a time interface.

To shed additional light on these numerical results, let us consider analytically the scattering of a wave by a time interface. First of all, in the more usual case of a spatial interface, an incident wave is partially reflected and transmitted. The incident, reflected, and transmitted waves have the same frequency but different wave numbers (wave vector in higher dimension). In the case of a single mode (i.e., a single band), scattering by a time interface transforms an earlier wave (mode prior to the change in parameter) into a later-backward and later-forward wave (mode after the change in parameter). The later waves have the same wave number (vector) as that of the earlier wave. The frequency is, however, not conserved. The frequencies of the later-forward and later-backward waves differ by their sign. Here, the normalized eigenvector of an early wave, for the initial coupling stiffness, α_i is given by

$$\vec{\hat{u}} = \begin{pmatrix} [\pm] y_1(\alpha_i) e^{ik2na} \\ y_2(\alpha_i) e^{ik(2n+1)a} \\ \pm y_3(\alpha_i) e^{ik2na} \\ \pm [\pm] y_4(\alpha_i) e^{ik(2n+1)a} \end{pmatrix} e^{i\omega t}. \tag{14}$$

We now consider the possibility of conversion into two modes (i.e., *intra*band and *inter*band scattering involving two different bands), for the final coupling stiffness, α_f, namely,

$$\begin{aligned} \vec{\hat{u}}'\{\pm\} &= \begin{pmatrix} [\pm] y_1(\alpha_f) e^{ik2na} \\ y_2(\alpha_f) e^{ik(2n+1)a} \\ \pm y_3(\alpha_f) e^{ik2na} \\ \pm [\pm] y_4(\alpha_f) e^{ik(2n+1)a} \end{pmatrix} e^{i\{\pm\}\omega' t} \text{ and} \\ \vec{\hat{u}}\{\pm\} &= \begin{pmatrix} [\mp] y_1(\alpha_f) e^{ik2na} \\ y_2(\alpha_f) e^{ik(2n+1)a} \\ \pm y_3(\alpha_f) e^{ik2na} \\ \pm [\mp] y_4(\alpha_f) e^{ik(2n+1)a} \end{pmatrix} e^{i\{\pm\}\omega t}. \end{aligned} \tag{15}$$

In Eq. (14) we have used $\{\pm\}$ to label the later-backward $\{-\}$ and later-forward $\{+\}$ waves. Note also the different bands associated with the $[\pm]$ and $[\mp]$.

The scattering process imposes continuity for the displacements of the four blocks in the unit cell [Eq. (16a)] as well as the continuity of the time derivative of the displacements [Eq. (16b)],

$$\begin{aligned} \vec{\hat{u}}(t=0) = \zeta' \vec{\hat{u}}'\{+\}(t=0) + \xi' \vec{\hat{u}}'\{-\}(t=0) \\ + \zeta'' \vec{\hat{u}}\{+\}(t=0) + \xi'' \vec{\hat{u}}\{-\}(t=0), \end{aligned} \tag{16a}$$

$$\begin{aligned} \omega \vec{\hat{u}}(t=0) = \omega' \zeta' \vec{\hat{u}}'\{+\}(t=0) - \omega' \xi' \vec{\hat{u}}'\{-\}(t=0) \\ + \omega \zeta'' \vec{\hat{u}}\{+\}(t=0) - \omega \xi'' \vec{\hat{u}}\{-\}(t=0). \end{aligned} \tag{16b}$$

Since y_3 is proportional to y_2 and y_4 to y_1, Eq. (16a) reduces to two equations involving only y_1's and y_2's. Similarly, Eq. (16b) reduced to two equations in y_1's and y_2's. We have therefore, four equations and four unknowns ζ', ξ', ζ'', and ξ''. The continuity conditions for this scattering problem can be written in the

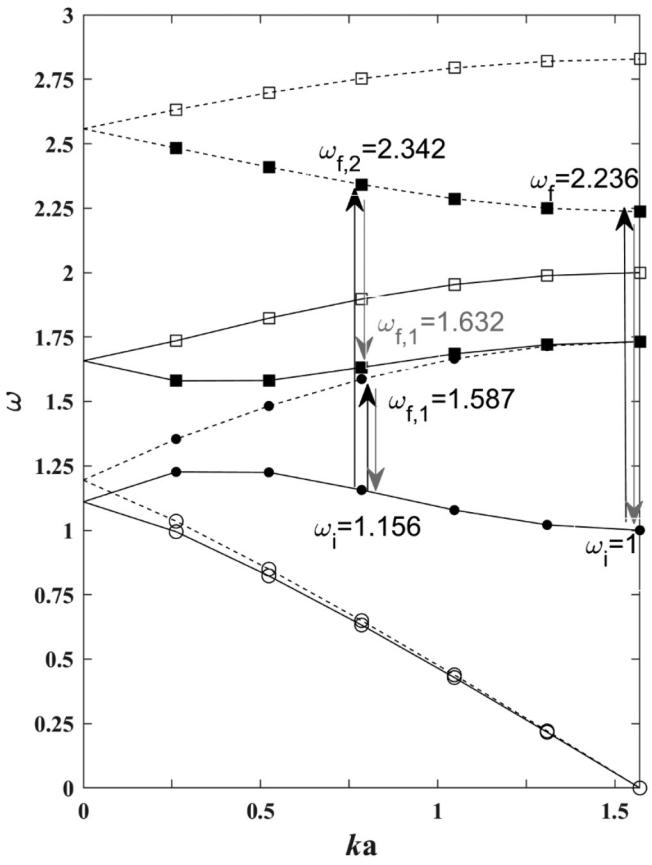

FIG. 6. Band structure of the simulated system for $\alpha = 0.5$ (solid lines) and $\alpha = 2.5$ (dashed lines). The ascending black arrows show the transitions resulting from scattering by a single time interface at the two wave numbers studied, $ka = \pi/4$ and $\pi/2$. ω_i and ω_f correspond to the initial (pre-scattering) and final (post-scattering) frequency. An additional index 1 or 2 is used when scattering excites two different modes. The descending grey arrows show the transitions due to scattering by a second time interface, which is part of a time defect.

following matrix form:

$$\begin{pmatrix} [\pm]y_1(\alpha_f) & [\pm]y_1(\alpha_f) & [\mp]y_1(\alpha_f) & [\mp]y_1(\alpha_f) \\ y_2(\alpha_f) & y_2(\alpha_f) & y_2(\alpha_f) & y_2(\alpha_f) \\ [\pm]y_1(\alpha_f)\omega' & -[\pm]y_1(\alpha_f)\omega' & [\mp]y_1(\alpha_f)\omega'' & -[\mp]y_1(\alpha_f)\omega'' \\ y_2(\alpha_f)\omega' & -y_2(\alpha_f)\omega' & y_2(\alpha_f)\omega'' & -y_2(\alpha_f)\omega'' \end{pmatrix} \begin{pmatrix} \zeta' \\ \xi' \\ \zeta'' \\ \xi'' \end{pmatrix} = \begin{pmatrix} [\pm]y_1(\alpha_i) \\ y_2(\alpha_i) \\ [\pm]y_1(\alpha_i)\omega \\ y_2(\alpha_i)\omega \end{pmatrix}. \tag{17}$$

This equation is applicable when both α_i and α_f are less or greater than $\beta_1 + \beta_2$ as well as when α_i or α_f are less or equal to $\beta_1 + \beta_2$. The definition of the bands corresponding to the eigenmodes given by Eqs. (14) and (15) involved in the scattering process depend on these conditions.

As long as $y_i(\alpha_f)'s$ are complex numbers different from $y_i(\alpha_i)$'s, scattering processes by a time interface involving simultaneously *intra*band and *inter*band transitions are allowed. This is what is observed in Fig. 5(a) when $ka = \pi/4$. Near the edge of the positive side of the BZ, at $ka = \pi/2$, we noted in Sec. 4 that $y_i(\alpha_i)$'s and $y_i(\alpha_f)$'s are independent of α_i and α_f. Let us consider the early mode with $([-], -)$ and $\alpha_i < \beta_1 + \beta_2$. We treat the problem of a sudden change of the coupling stiffness to a value $\alpha_f > \beta_1 + \beta_2$. This is the case of Fig. 3 as well as the numerical simulation of Fig. 5(b). We have $y_1(\alpha_i) = 1/2\sqrt{2}\sqrt{i}$ and $y_2(\alpha_i) = 1/2\sqrt{2}\sqrt{-i}$; $y_1(\alpha_f) = -1/2\sqrt{2}\sqrt{-i}$ and $y_2(\alpha_f) = -1/2\sqrt{2}\sqrt{i}$. Under these conditions, after some algebraic manipulations, Eq. (17) reduces to $\begin{pmatrix} 1 & 1 & -1 & -1 \\ 1 & 1 & 1 & 1 \\ r' & -r' & -r'' & r'' \\ r' & -r' & r'' & -r'' \end{pmatrix} \begin{pmatrix} \zeta' \\ \xi' \\ \zeta'' \\ \xi'' \end{pmatrix} = i \begin{pmatrix} 1 \\ 1 \\ 1 \\ 1 \end{pmatrix}$, where $r' = \omega'/\omega$ and $r'' = \omega'/\omega$. This system of equations leads to the solution $\begin{pmatrix} \zeta' \\ \xi' \\ \zeta'' \\ \xi'' \end{pmatrix} = i/2 \begin{pmatrix} 1 + 1/r' \\ 1 - 1/r' \\ 0 \\ 0 \end{pmatrix}$. Since the early state was for the band with $[-]$, and the only single later state corresponds also to $[-]$, and since the time interface considered here involved band inversion ($\alpha_i < \beta_1 + \beta_2$ and $\alpha_f > \beta_1 + \beta_2$), the scattering process corresponds to an *inter*band transition. This phenomenon was reported in Fig. 5(b). A similar argument can be utilized to explain the result of Fig. 5(c).

These striking results motivated us to carry out another set of numerical simulations, where instead of keeping the final coupling parameter α_f constant throughout the remaining 2^{17} time steps of the simulation, the coupling stiffness is changed again back to the initial value α_i. This corresponds to two subsequent time interfaces. With this process, α_f is localized in time, realizing a time defect equivalent to a Fabry–Pérot cavity in time. The time duration over which the coupling stiffness retains the value α_f is chosen to be a single cycle of the early wave. Simulations with time defects lasting 5 and 10 cycles showed the same behavior as that for one cycle. We have recorded the displacement field of a representative block element in the top chain and calculated the power spectral density via a temporal Fourier transform. We investigate the same three combinations of ka, and (α_i, α_f) as in the case of a single time interface. Results of the scattering by the localized time defect are presented in Fig. 7. At the wave number, $ka = \pi/4$, the first time interface scatters the earlier wave of frequency $\omega_i = 1.156$ (second band in the positive sector of the BZ) into the superposition of two waves with frequencies $\omega_{f,1} = 1.587$ and $\omega_{f,2} = 2.342$ (second and third bands in the positive half of the BZ) as was shown in Fig. 5(a). Scattering by the second interface converts these two waves back into the earlier wave (second band in the positive half of the band structure) but also now a wave with a frequency of 1.632 corresponding to the third band (in the positive half of the BZ) when the coupling stiffness is α_i. Figure 6 also includes illustrations of these scattering processes. For $ka = \pi/2$, the initial single mode is preserved and remains insensitive to the presence of the

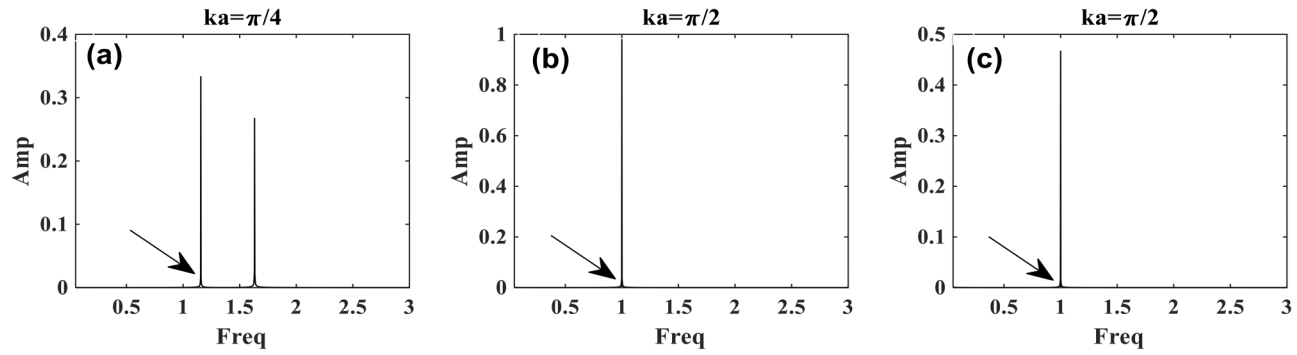

FIG. 7. Power spectral density of the displacement of a representative rotator in the top chain, showing the eigenfrequencies. Arrows indicate the initial excitation frequency (ω_i) of the input eigenmode: (a) $\omega_i = 1.156$ and $(\alpha_i, \alpha_f) = (0.5, 2.5)$, (b) $\omega_i = 1.0$ and $(\alpha_i, \alpha_f) = (0.5, 2.5)$, and (c) $\omega_i = 1.0$ and $(\alpha_i, \alpha_f) = (0.5, 2.5)$. System parameters: $N_c = 12$, $N_m = 2$, $\beta_1 = 0.5$, $\beta_2 = 1.0$.

time defect. Such robustness occurs regardless of the magnitude of the variation of coupling stiffness forming the time defect [from $\alpha_i = 0.5$ to $\alpha_f = 1.0$ (Fig. 6(b)] or from $\alpha_i = 0.5$ to $\alpha_f = 2.5$ [Fig. 5(c)], that is, with or without band inversion).

The phenomenon of scattering by a time interface or a time defect observed here for $ka \neq \pi/2$ could be realized in any general two band system as long as the eigenvectors depend on a physical parameter such as stiffness. However, the unique nature of the eigenvector of the coupled chains system at $ka = \pi/2$ leads to the observed transition restriction preserving the initial single mode.

While, we have considered discrete time interfaces by sudden changes in the strength of the coupling parameter, other temporal and/or spatial variations in the coupling parameter such as periodic spatiotemporal modulation of the stiffness[7] could lead to other forms of synthetic dimensions. Such dynamic periodic modulations of stiffness could be used to create modes at different frequencies and realize an additional one-dimensional lattice in a synthetic frequency dimension.

VI. CONCLUSION

We have introduced a model system composed of elastically coupled one-dimensional chains of elastic rotators. The two chains forming the coupled system are analogous to SSH models. We demonstrate analytically and numerically that this system supports an exceptional number of topological properties such as Dirac degeneracies, band inversion, and topological transition as the strength of the coupling parameter is varied, nonseparability of the modes' degrees of freedom along and across the coupled chains and synthetic dimension via tuning of the parameter coupling the chains. When coupling two topologically distinct SSH-like rotator chains (i.e., the chains are translated by half a spatial period), the elastic band structure exhibits two Dirac degeneracies at the origin of the BZ. The band structure undergoes band inversion upon variations in the strength of the stiffness of the springs coupling the chains. Band inversion leads to a discrete change in the Berry phase associated with the individual dispersion relations. The coupled system with topologically distinct chains supports elastic modes that are nonseparable in the 4D Hilbert space product of the 2D Hilbert space of the position of the rotators within the unit cell of individual chains and the 2D Hilbert space of the chains. This characteristic is in contrast with a coupled system with topologically identical chains (the chains are in perfect registry along their length) for which there are no Dirac points and the degrees of freedom along and across the coupled chains are separable. By varying the strength of the stiffness of the coupling parameter in a cyclic manner[43] or discontinuous manner[44] may extend the system with a synthetic dimension possibly enabling the exploration the topological properties of the systems within a higher-dimensional synthetic space. Varying the coupling parameter in time, leads to scattering by time interfaces, enabling transitions between eigenmodes.

This work shows that by exploiting the analogies between TA and quantum mechanics, one can harness mode quantization (via discrete changes in Berry phase), coherent nonseparable modes reminiscent of entangled states to overcome stability and scalability challenges of true quantum systems in massive data information processing—within the context of the second quantum revolution. Furthermore, by combining synthetic dimensions with the geometric dimensions to form higher-dimensional synthetic space one can access arbitrary geometries and potentials that are unavailable in real space lattices. Coupling between degrees of freedom in geometric and synthetic spaces may lead to even more exotic features than the one described herein. These properties may include non-local long range order characteristic of topological phases of matter.[45]

APPENDIX: COUPLED CHAINS IN REGISTRY

Here, we consider a slight variation of the system of Fig. 1, where now the stiffnesses β_1 and β_2 for both coupled chains are in registry (i.e., the same stiffnesses face each other between the two chains). In contrast to the model of Fig. 1, the coupled chains in registry are topologically equivalent. The Berry phase of two individual chains in registry differs by 0 or 2π.[3] The rotational

equations of motion of this new system take the form

$$m\frac{\partial^2 u_{2n}}{\partial t^2} = -\beta_2(u_{2n-1}+u_{2n}) - \beta_1(u_{2n}-u_{2n+1}) + \alpha(v_{2n}-u_{2n}), \tag{A1a}$$

$$m\frac{\partial^2 u_{2n+1}}{\partial t^2} = \beta_1(u_{2n}-u_{2n+1}) - \beta_2(u_{2n+1}+u_{2n+2}) + \alpha(v_{2n+1}-u_{2n+1}), \tag{A1b}$$

$$m\frac{\partial^2 v_{2n}}{\partial t^2} = -\beta_2(v_{2n-1}+v_{2n}) - \beta_1(v_{2n}-v_{2n+1}) - \alpha(v_{2n}-u_{2n}), \tag{A1c}$$

$$m\frac{\partial^2 v_{2n+1}}{\partial t^2} = \beta_1(v_{2n}-v_{2n+1}) - \beta_2(v_{2n+1}+v_{2n+2}) - \alpha(v_{2n+1}-u_{2n+1}). \tag{A1d}$$

Similarly to Sec. 2, we choose an Ansatz to solve these equations in the form $u_{2n} = A_1' e^{ik2na} e^{i\omega t}$, $u_{2n+1} = A_2' e^{ik(2n+1)a} e^{i\omega t}$, $v_{2n} = B_1' e^{ik2na} e^{i\omega t}$, and $v_{2n+1} = B_2' e^{ik(2n+1)a} e^{i\omega t}$. Equations (A1a), (A1b), (A1c), and (A1d) reduce to an eigenproblem of the form

$$\overleftrightarrow{D}'\vec{A}' = 0, \tag{A2}$$

where

$$\overleftrightarrow{D}' = \begin{pmatrix} \gamma & -\delta & -\alpha & 0 \\ -\delta^* & \gamma & 0 & -\alpha \\ -\alpha & 0 & \gamma & -\delta \\ 0 & -\alpha & -\delta^* & \gamma \end{pmatrix} \text{ and } \vec{A}' = \begin{pmatrix} A_1' \\ A_2' \\ B_1' \\ B_2' \end{pmatrix},$$

with $\gamma = -m\omega^2 + \beta_1 + \beta_2 + \alpha$ and $\delta = \beta_1 e^{+ika} - \beta_2 e^{-ika}$. Again, δ^* is the complex conjugate of δ. Equation (A2) can be rewritten as

$$(\overleftrightarrow{M} + \alpha\overleftrightarrow{C})\vec{A}' = 0, \tag{A3}$$

where we have introduced the matrices

$$\overleftrightarrow{M} = \begin{pmatrix} \gamma_0 & -\delta & 0 & 0 \\ -\delta^* & \gamma_0 & 0 & 0 \\ 0 & 0 & \gamma_0 & -\delta \\ 0 & 0 & -\delta^* & \gamma_0 \end{pmatrix} \text{ and}$$

$$\overleftrightarrow{C} = \begin{pmatrix} 1 & 0 & -1 & 0 \\ 0 & 1 & 0 & -1 \\ -1 & 0 & 1 & 0 \\ 0 & -1 & 0 & 1 \end{pmatrix}.$$

Here, $\gamma_0 = -m\omega^2 + \beta_1 + \beta_2$. We note that these 4×4 matrices can be expressed as a tensor product of two 2×2 matrices, such that

$\overleftrightarrow{M} = \overleftrightarrow{N} \otimes \overleftrightarrow{I}$ with $\overleftrightarrow{N} = \begin{pmatrix} \gamma_0 & -\delta \\ -\delta^* & \gamma_0 \end{pmatrix}$ and $\overleftrightarrow{C} = \overleftrightarrow{I} \otimes \overleftrightarrow{c}$ with $\overleftrightarrow{c} = \begin{pmatrix} 1 & -1 \\ -1 & 0 \end{pmatrix}$. Equation (A3) is then replaced by

$$(\overleftrightarrow{N} \otimes \overleftrightarrow{I} + \alpha\overleftrightarrow{I} \otimes \overleftrightarrow{c})\vec{A}' = 0. \tag{A4}$$

The form of Eq. (A4) enables us to seek solutions for the amplitude vector expressed as tensor products of two 2×1 vectors, namely, $\vec{A}' = \vec{s} \otimes \vec{e}$. With this type of solution, Eq. (A4) becomes

$$(\overleftrightarrow{N}\vec{s}) \otimes (\overleftrightarrow{I}\vec{e}) + \alpha(\overleftrightarrow{I}\vec{s}) \otimes (\overleftrightarrow{c}\vec{e}) = 0. \tag{A5}$$

If we choose $\vec{e}$ to be an eigenvector of the matrix $\overleftrightarrow{c}$, that is, $\vec{e}_1 = 1/\sqrt{2}\begin{pmatrix} 1 \\ 1 \end{pmatrix}$ (with eigenvalue $\lambda_1 = 0$) and $\vec{e}_2 = 1/\sqrt{2}\begin{pmatrix} 1 \\ -1 \end{pmatrix}$ (with eigenvalue $\lambda_2 = 2$), then Eq. (A5) can be separated as

$$[(\overleftrightarrow{N} + \alpha\lambda_n\overleftrightarrow{I})\vec{s}] \otimes (\overleftrightarrow{I}\vec{e}_n) = 0. \tag{A6}$$

Since $\overleftrightarrow{I}\vec{e}_n \neq 0$, $\vec{s}$ is a solution of $(\overleftrightarrow{N} + \alpha\lambda_n\overleftrightarrow{I})\vec{s} = 0$. The dispersion relations are given by $m\omega^2 = \beta_1 + \beta_2 + \lambda_n\alpha[\pm]\sqrt{\beta_1^2 + \beta_2^2 + 2\beta_1\beta_2\cos 2ka}$. The four bands do not cross anywhere within the BZ.

The amplitude vector for the system with β_1 and β_2 in registry between the two coupled chains is in the form of the tensor product $\vec{A}' = \vec{s} \otimes \vec{e}$. In the language of quantum mechanics, this amplitude vector is separable. The 2×1 vector $\vec{s}$ spans the Hilbert space of the position of the two rotator block elements in a unit cell. The 2×1 vector $\vec{e}$ spans the Hilbert space of the chains. $\vec{e}$ sets the relative phase between blocks in the same unit cell belonging to the different chains.

ACKNOWLEDGMENTS

This research was funded by the National Science Foundation Emerging Frontiers in Research and Innovation (EFRI) Award (No. 1640860).

DATA AVAILABILITY

The data that support the findings of this study are available from the corresponding author upon reasonable request.

REFERENCES

[1]G. Ma, M. Xiao, and C. T. Chan, "Topological phases in acoustic and mechanical systems," Nat. Rev. Phys. **1**, 281 (2019).
[2]J. Yin, M. Ruzzene, J. Wen, D. Yu, L. Cai, and L. Yue, "Band transition and topological interface modes in 1D elastic phononic crystals," Sci. Rep. **8**, 6806 (2018).
[3]M. Arif Hasan, L. Calderın, K. Runge, and P. A. Deymier, "Spectral analysis of amplitudes and phases of lattice vibrations: Topological applications," J. Acoust. Soc. Am. **146**, 748 (2019).
[4]R. Fleury, D. L. Sounas, and A. Alù, "Subwavelength ultrasonic circulator based on spatiotemporal modulation," Phys. Rev. B **91**, 174306 (2015).
[5]M. Xiao, G. Ma, Z. Yang, P. Sheng, Z. Q. Zhang, and C. T. Chan, "Geometric phase and band inversion in periodic acoustic systems," Nat. Phys. **11**, 240 (2015).

[6]P. A. Deymier, K. Runge, and J. O. Vasseur, "Geometric phase and topology of elastic oscillations and vibrations in model systems: Harmonic oscillator and superlattice," AIP Adv. **6**, 121801 (2016).
[7]N. Swinteck, S. Matsuo, K. Runge, J. O. Vasseur, P. Lucas, and P. A. Deymier, "Bulk elastic waves with unidirectional backscattering-immune topological states in a time-dependent superlattice," J. Appl. Phys. **118**, 063103 (2015).
[8]G. Trainiti and M. Ruzzene, "Non-reciprocal elastic wave propagation in spatio-temporal periodic structures," New J. Phys. **18**, 083047 (2016).
[9]Y. Chen, X. Li, H. Nassar, A. N. Norris, C. Daraio, and G. Huang, "Nonreciprocal wave propagation in a continuum-based metamaterial with space-time modulated resonators," Phys. Rev. Appl. **11**, 064052 (2019).
[10]P. A. Deymier, V. Gole, P. Lucas, J. O. Vasseur, and K. Runge, "Tailoring phonon band structures with broken symmetry by shaping spatiotemporal modulations of stiffness in a one-dimensional elastic waveguide," Phys. Rev. B **96**, 064304 (2017).
[11]M. A. Hasan, L. Calderin, T. Lata, P. Lucas, K. Runge, and P. A. Deymier, "The sound of Bell states," Commun. Phys. **2**(1), 106 (2019).
[12]P. A. Deymier, M. A. Hasan, and K. Runge, "Navigating the Hilbert space of nonseparable elastic states in arrays of periodically coupled one-dimensional waveguides," AIP Adv. **10**, 095101 (2020).
[13]P. A. Deymier, K. Runge, and M. A. Hasan, "Exponentially complex nonseparable states in planar arrays of nonlinearly coupled one-dimensional elastic waveguides," J. Phys. Commun. **4**, 085018 (2020).
[14]P. Wang, L. Lu, and K. Bertoldi, "Topological phononic crystals with one-way elastic edge waves," Phys. Rev. Lett. **115**, 104302 (2015).
[15]R. K. Pal, M. Schaeffer, and M. Ruzzene, "Helical edge states and topological phase transitions in phononic systems using bi-layered lattices," J. Appl. Phys. **119**, 084305 (2016).
[16]R. K. Pal and M. Ruzzene, "Edge waves in plates with resonators: An elastic analogue of the quantum valley Hall effect," New J. Phys. **19**, 025001 (2017).
[17]H. Ge, X. Ni, Y. Tian, S. K. Gupta *et al.*, "Experimental observation of acoustic Weyl points and topological surface states," Phys. Rev. Appl. **10**, 014017 (2018).
[18]F. Li, X. Huang, J. Lu, J. Ma, and Z. Liu, "Weyl points and fermi arcs in a chiral phononic crystal," Nat. Phys. **14**, 30–34 (2018).
[19]M. Xiao, W.-J. Chen, W.-Y. He, and C. T. Chan, "Synthetic gauge flux and Weyl points in acoustic systems," Nat. Phys. **11**, 920–924 (2015).
[20]S. S. Ganti, T.-W. Liu, and F. Semperlotti, "Weyl points and topological surface states in a three-dimensional elastic lattice," New J. Phys. **22**, 083001 (2020).
[21]M. Z. Hasan and C. L. Kane, "Topological insulators," Rev. Mod. Phys. **82**, 3045 (2010).
[22]E. Lustig, S. Weimann, Y. Plotnik, Y. Lumer, M. A. Bandress, A. Szameit, and M. Segev, "Photonic topological insulator in synthetic dimensions," Nature **567**, 356 (2019).
[23]L. Yuan, Q. Lin, M. Xia, and S. Fan, "Synthetic dimension in photonics," Optica **5**, 1396 (2018).
[24]C. Li, S. Lin, G. Zhang, and Z. Song, "Topological nodal points in two coupled Su-Schrieffer-Heeger chains," Phys. Rev. B **96**, 125418 (2017).
[25]J.-W. Rhim, J. H. Bardarson, and R.-J. Slager, "Unified bulk-boundary correspondence for band insulators," Phys. Rev. B **97**, 115153 (2018).
[26]K. Padavić, S. S. Hegde, W. DeGottardi, and S. Vishveshwara, "Topological phases, edges modes, and the Hofstadter butterfly in coupled Su-Schrieffer-Heeger systems," Phys. Rev. B **98**, 024205 (2018).
[27]E. Prodan, K. Dobiszewski, A. Kanwal, J. Palmieri, and C. Prodan, "Dynamical Majorana edge modes in a broad class of topological mechanical systems," Nat. Commun. **8**, 14587 (2017).
[28]R. Chaunsali, E. Kim, A. Thakkar, P. G. Kevrekidis, and J. Yang, "Demonstrating an *in situ* topological band transition in cylindrical granular chains," Phys. Rev. Lett. **119**, 024301 (2017).
[29]J. Köpfler, T. Frenzel, M. Kadic, J. Schmalian, and M. Wegener, "Topologically protected twist edge states for a resonant mechanical laser-beam scanner," Phys. Rev. Appl. **11**, 034059 (2019).
[30]A. Vasiliev, A. E. Miroshnichenko, and M. Ruzzene, "A discrete model and analysis of one-dimensional deformations in a structural interface with micro-rotations," Mech. Res. Commun. **37**, 225 (2010).
[31]A. Vasiliev, A. Miroshnichenko, and M. Ruzzene, "Multifield model for Cosserat media," J. Mech. Mater. **3**, 1365 (2008).
[32]E. Cosserat and F. Cosserat, *Théorie des Corps Déformables* (Hermann et Fils, Paris, 1909).
[33]M. V. Berry, "Quantal phase factors accompanying adiabatic changes," Proc. R. Soc. Lond. A **392**, 45 (1984).
[34]J. Zak, "Berry's phase for energy bands in solids," Phys. Rev. Lett. **62**, 2747 (1989).
[35]R. Verba, I. Lisenkov, I. Krivorotov, V. Tiberkevich, and A. Slavin, "Nonreciprocal surface acoustic waves in multilayers with magnetoelastic and interfacial Dzyaloshinskii-Moriya interactions," Phys. Rev. Appl. **9**, 064014 (2018).
[36]Y. Wang, B. Yousefzadeh, H. Chen, H. Nassar, G. Huang, and C. Daraio, "Observation of nonreciprocal wave propagation in a dynamic phononic lattice," Phys. Rev. Lett. **121**, 194301 (2018).
[37]M. S. Kang, A. Butsch, and P. S. J. Russell, "Reconfigurable light-driven opto-acoustic isolators in photonic crystal fibre," Nat. Photonics **5**, 549 (2011).
[38]G. Trainiti, Y. Xia, J. Marconi, G. Cazzulani, A. Erturk, and M. Ruzzene, "Time-periodic stiffness modulation in elastic metamaterials for selective wave filtering: Theory and experiment," Phys. Rev. Lett. **122**, 124301 (2019).
[39]R. E. Simpson, P. Fons, A. V. Kolobov, T. Fukaya *et al.*, "Interfacial phase-change memory," Nat. Nanotechnol. **6**, 501 (2011).
[40]J. T. Mendonça, A. Guerreiro, and A. M. Martins, "Quantum theory of time refraction," Phys. Rev. A **62**, 033805 (2000).
[41]C. Caloz and Z.-L. Deck-Léger, "Spacetime metamaterials—Part I: General concepts," IEEE Trans. Antennas Propag. **68**, 1569 (2020).
[42]C. Caloz and Z.-L. Deck-Léger, "Spacetime metamaterials—Part II: Theory and applications," IEEE Trans. Antennas Propag. **68**, 1583 (2020).
[43]L. Li, Z. Xu, and S. Chen, "Topological phases of generalized Su-Schrieffer-Heeger models," Phys. Rev. B **89**, 085111 (2014).
[44]S. V. Silva, D. E. Fernandes, T. A. Morgado, and M. G. Silveirinha, "Fractional Chern numbers and topological pumping in photonic systems," arXiv:1912.11271v2 (2020).
[45]P. A. Deymier and K. Runge, "Evidence for hidden order in a nonlimnear model elastic system," J. Phys. Condens. Matter **31**, 10LT01 (2019).